Aust. J. Phys., 1986, **39**, 679–85

Relativistic Effects in the Photoionisation of Heavy Atoms: Cooper Minima*

Pranawa C. Deshmukh,[A] *B. R. Tambe*[B] *and Steven T. Manson*[C]

[A] Department of Physics, Indian Institute of Technology, Madras 600 0036, India.
[B] Department of Physics, Southern Technical Institute, Marietta, GA 30060, U.S.A.
[C] Department of Physics and Astronomy, Georgia State University, Atlanta, GA 30303, U.S.A.

Abstract

Cooper minima are known to profoundly affect photoionisation cross sections. They become particularly important in high-Z atoms where relativistic effects split each nonrelativistic Cooper minimum into three minima (two for s states). In addition, there are significant splittings in these 'triplets'. In this paper, the systematics of these relativistic Cooper minima are explored, over a broad range of elements, for 5p, 5d, 6s and 6p subshells. The phenomenology is presented and the physics behind the results discussed. In addition, the important implications for branching rates and photoelectron angular distributions are presented.

1. Introduction

Over the past two decades, our understanding of the overall systematics of the photoionisation of low-Z atoms has mushroomed, largely through the interplay between theory and experiment (Fano and Cooper 1968; Manson 1976, 1977; Wuilleumier 1976; Starace 1981; Samson 1981). The calculations, however, have been largely nonrelativistic. Thus, their ability to deal with high-Z atoms, where relativistic effects become important and experimental data are sparse, is somewhat questionable. Thus, it is clear, that relativistic calculations are needed, and we have embarked on such a program.

Relativistic interactions affect the photoionisation of high-Z atoms in a number of ways. In this work we have sought to uncover which aspect(s) of the relativistic interactions are most important to photoionisation. To this end, we have focused our study on the feature of photoionisation cross sections which is, perhaps, most sensitive to the details of the calculation, the Cooper minimum (Cooper 1962; Manson and Cooper 1968). This minimum, perhaps more accurately called a Ditchburn–Bates–Seaton–Cooper minimum, is characterised by a photon energy for which the dipole matrix element for the dominant $l \rightarrow l+1$ channel has a zero. These zeros occur extensively for outer and near-outer subshells throughout the periodic system (Manson 1985). It is important to note that a single nonrelativistic zero splits into three (two for initial s states) under the influence of the spin–orbit interaction; for

* Paper presented at the Specialist Workshop on Excited and Ionised States of Atoms and Molecules, Strathgordon, Tasmania, 3–7 February 1986.

0004-9506/86/050679$02.00

example, a nonrelativistic p → d channel splits into $p_{3/2} \rightarrow d_{3/2}$, $p_{3/2} \rightarrow d_{5/2}$ and $p_{1/2} \rightarrow d_{3/2}$ relativistic channels, each having its own Cooper minimum (zero) at a different energy.

In this paper we present and compare results for 5p, 5d, 6s and 6p subshells over a range of Z values. Calculations were performed using simple Hartree–Slater (HS) wavefunctions (Herman and Skillman 1963) for the nonrelativistic case, and Dirac–Slater (DS) wavefunctions for the relativistic case. Using the same atomic model in each case, with the HS calculations based on the Schrödinger equation and the DS calculations based on the Dirac equation, we could then elucidate the effects specifically due to relativistic interactions. The details of these calculations have been given by Manson and Cooper (1968) and by Tambe and Manson (1984).

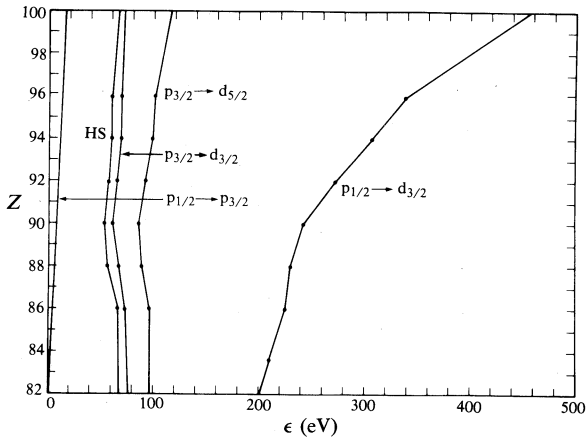

Fig. 1. Trajectory (in photoelectron energy) of the 'Cooper' zeros in the 6p → d dipole matrix elements, as a function of Z. The relativistic matrix elements are labelled, while HS refers to the nonrelativistic Hartree–Slater results. Also shown, for comparison, is the spin–orbit splitting of the $6p_{1/2}$–$6p_{3/2}$ energy levels as a function of Z.

2. Results and Discussion

The results for the 6p → d Cooper minima are given in Fig. 1 (Manson *et al.* 1983), where the trajectories of each of the relativistic and nonrelativistic minima are shown as a function of Z. There are several striking features in these results. First, we note the strong Z dependence of the $6p_{1/2} \rightarrow \epsilon d_{3/2}$ minimum; for $Z = 82$ it is located about 200 eV above threshold, while by $Z = 100$ it appears about 460 eV above threshold. Second, the energy splitting between the $6p_{3/2}$ and $6p_{1/2}$ minima is huge, being 100 eV for $Z = 82$ and increasing to more than 300 eV by $Z = 100$. There is also a splitting between the $6p_{3/2} \rightarrow \epsilon d_{3/2}$ and $6p_{3/2} \rightarrow \epsilon d_{5/2}$ minima which increases slowly from about 20 eV at $Z = 82$ to almost 50 eV at $Z = 100$, as can be seen from Fig. 1. Further, the locus of the nonrelativistic p → d minima lies below any of the relativistic minima, roughly a constant 10 eV below the $p_{3/2} \rightarrow d_{3/2}$ minima independent of Z. Thus the effect of relativistic interactions is both to move the minima to higher energy and to introduce a very significant energy splitting among them.

To understand these results, we consider first the $p_{1/2} \rightarrow d_{3/2}$ and $p_{3/2} \rightarrow d_{3/2}$ minima. In our DS calculation for a given photoelectron energy ϵ, the $\epsilon d_{3/2}$ wavefunction is exactly the same, independent of the initial state of the photoelectron. Thus, since the final state in each of these transitions is exactly the same, the huge splitting must result from the differences between the $6p_{1/2}$ and $6p_{3/2}$ bound-state wavefunctions. In a first approximation, in regions where these wavefunctions are large, the $6p_{1/2}$ wavefunction is the same as that of $6p_{3/2}$ only displaced inward towards the nucleus, because the spin–orbit force is attractive for $j = l - \frac{1}{2}$ but repulsive for $j = l + \frac{1}{2}$. Thus at the energy for which the overlap of the $6p_{3/2}$ wavefunction is such that the dipole matrix element vanishes, the radial extent of the $\epsilon d_{3/2}$ wavefunction is still too great to have the similar overlap needed for the $6p_{1/2}$ matrix element to vanish. Since continuum wavefunctions move in with increasing energy, it is clear that the $6p_{1/2}$ minimum will occur at a higher energy.

The $6p_{1/2}$–$6p_{3/2}$ spin–orbit splitting of bound-state energies, also shown in Fig. 1, is an order of magnitude smaller than the splitting of the minima. One might think that the same energy difference by which the discrete $p_{1/2}$ wavefunction is displaced inward from that of $p_{3/2}$ should cause $\epsilon d_{3/2}$ to move in similarly, so that the minima would be split by about the same amount as the discrete states. This is not true, owing to the centrifugal barrier for d waves which makes it far more difficult for continuum d waves to penetrate the core region than for the discrete p orbitals. The strength of the centrifugal barrier for d waves, then, is responsible for the more than tenfold 'magnification' of the splitting, while the increasing strength of the spin–orbit interaction as Z increases causes the increased splitting of the minima with Z.

We see from Fig. 1 that the location of the $6p_{3/2} \rightarrow \epsilon d_{3/2}$ zero varies little with Z while, as already noted, the $6p_{1/2} \rightarrow \epsilon d_{3/2}$ zero shows an extremely strong variation. In examining this difference, we have observed that both 6p wavefunctions move in by about the same amount with increasing Z, with the displacement of $6p_{1/2}$ inward with respect to $6p_{3/2}$ remaining roughly constant. (Although the $6p_{1/2}$–$6p_{3/2}$ spin–orbit energy splitting increases with increasing Z, it also takes a larger energy to displace the wavefunctions as they move toward the interior of the atoms where the potential is larger.) The d wavefunctions are also displaced inward with increasing Z, and just enough so that the $6p_{3/2} \rightarrow \epsilon d_{3/2}$ minimum has very little variation with Z. Then, although the $\epsilon d_{3/2}$ wavefunction moves in the same distance for each Z to reach the point where the $6p_{1/2} \rightarrow \epsilon d_{3/2}$ matrix element vanishes, since the 6p wavefunctions are displaced inward with increasing Z it takes progressively more energy for the $\epsilon d_{3/2}$ wavefunction to move in that same distance owing to the strength of the d-wave potential barrier. Thus a given energy increase has a greater effect on the $\epsilon d_{3/2}$ wavefunction in the vicinity of the $6p_{3/2}$ minimum than near the $6p_{1/2}$ minimum, which occurs when the continuum wavefunction is closer in.

The much smaller splitting between the $6p_{3/2} \rightarrow \epsilon d_{3/2}$ and $6p_{3/2} \rightarrow \epsilon d_{5/2}$ minima is evidently due to the final continuum states, since the initial states are exactly the same. The spin–orbit force pulls the $\epsilon d_{3/2}$ wavefunction in and pushes $\epsilon d_{5/2}$ out; thus, the $\epsilon d_{3/2}$ minimum occurs at lower energy, as seen in Fig. 1. In addition, the increase in the strength of the spin–orbit interaction with Z causes the increase in the separation of this minima with Z.

Finally, we note that the nonrelativistic $6p \rightarrow \epsilon d$ minimum behaves almost exactly like the $6p_{3/2} \rightarrow \epsilon d_{3/2}$ minimum, as a function of Z. Owing to the relativistic contraction of the core, the electrostatic attraction becomes greater for p states and

less for d states, compared with nonrelativistic values (Manson *et al.* 1983). But, the $6p_{3/2}$ wavefunction also 'feels' a spin–orbit repulsion which renders its net attraction approximately nonrelativistic, while $\epsilon d_{3/2}$ 'feels' a spin–orbit attraction, so that its net attraction is also approximately nonrelativistic.

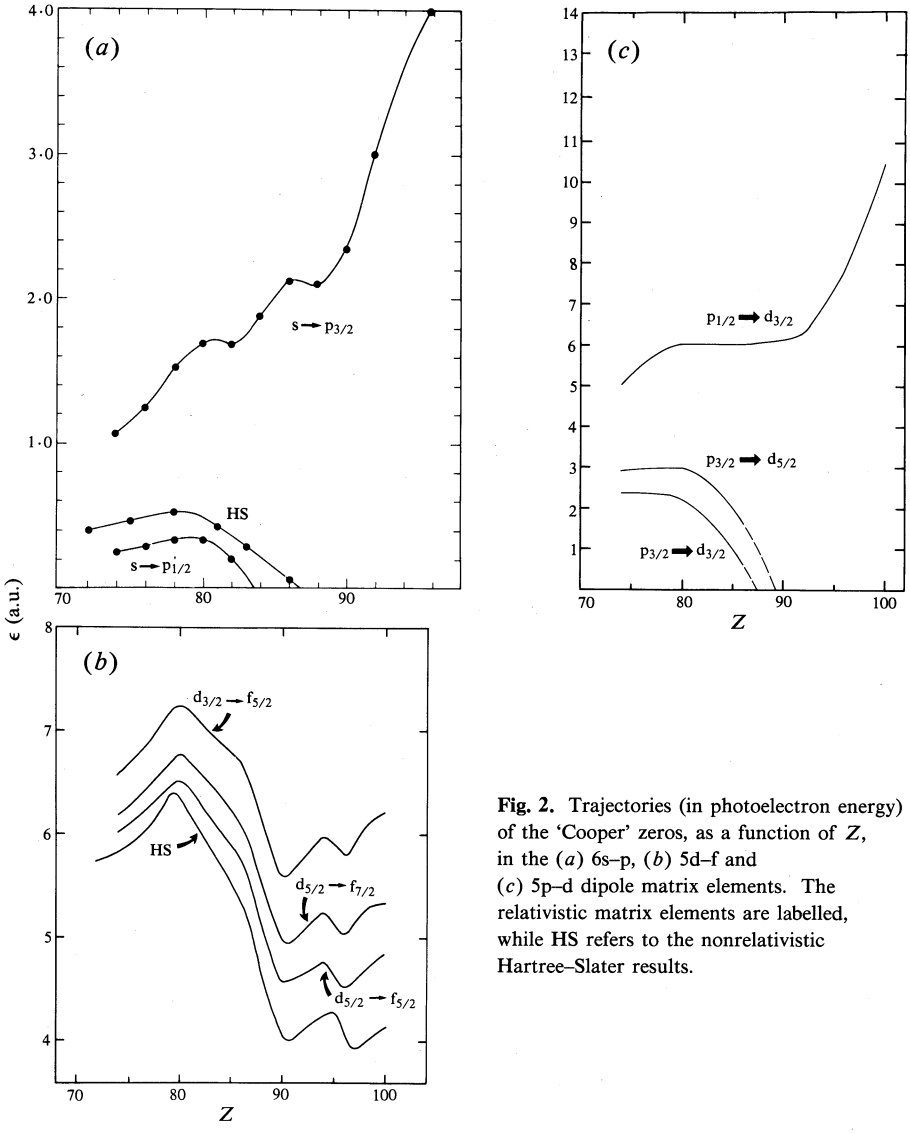

Fig. 2. Trajectories (in photoelectron energy) of the 'Cooper' zeros, as a function of Z, in the (*a*) 6s–p, (*b*) 5d–f and (*c*) 5p–d dipole matrix elements. The relativistic matrix elements are labelled, while HS refers to the nonrelativistic Hartree–Slater results.

A similar result is found for the 6s subshell shown in Fig. 2*a*. In this case the 6s $\rightarrow \epsilon p_{1/2}$ zero moves below threshold by $Z = 84$, while the 6s $\rightarrow \epsilon p_{3/2}$ zero is moving toward higher energies. Basically, the 6s and $\epsilon p_{1/2}$ wavefunctions both contract under the action of relativity (as discussed above) so that this transition is rather similar to the nonrelativistic HS result, also shown. The outward movement of the 6s $\rightarrow \epsilon p_{3/2}$ zero is because the spin–orbit force is repulsive for a $p_{3/2}$ state; the situation is quite similar to the $6p_{1/2} \rightarrow \epsilon d_{3/2}$ transition discussed above.

The situation for the 5d subshell (Tambe and Manson 1984), shown in Fig. 2*b*, is similar to the 6p case, with one important exception; the energy scale of the splitting of these zero trajectories is much smaller. This is due to the fact that spin–orbit splittings become smaller with increasing l. Below $Z = 80$, the zeros move out because the 5d discrete orbitals are contracting with increasing Z, while the continuum f state is not. The zero moves to lower energies in all of the relativistic channels, as well as the nonrelativistic channel, in the range $Z = 80$–90, indicative of the contraction of the f wave in this region. This contraction is more rapid than the discrete 5d contraction, leading to a net moving in of the zero. At still higher Z values the behaviour of the trajectories is obscured by wiggles which are of small amplitude, but real. They are due to the irregular filling of the 6d subshell as compared with the 5f subshell in this region. However, if regular filling is assumed, they disappear (Tambe and Manson 1984). Thus, ignoring them, it is seen that the $d_{5/2}$ zeros remain at a fairly constant energy, while the $d_{3/2}$ zero is moved to larger energy, with increasing Z, similar to the 6p case.

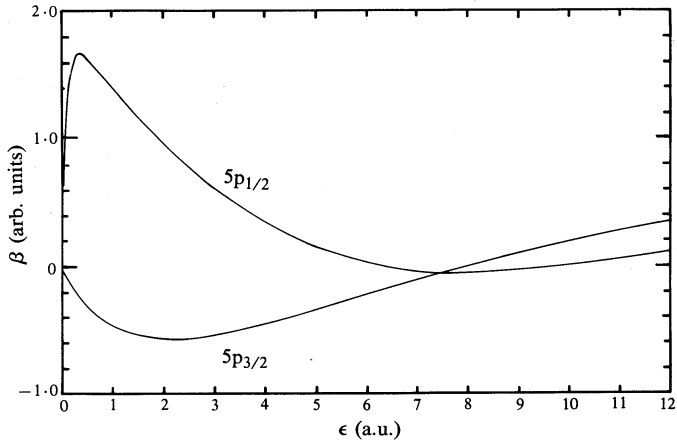

Fig. 3. Photoelectron angular distribution asymmetry parameter β for the $5p_{1/2}$ and $5p_{3/2}$ subshells of uranium.

The results for the 5p photoionisation are shown in Fig. 2*c*. These again are very similar to the 6p results, with a very important exception; by $Z = 90$ the $p_{3/2}$ zeros have moved below threshold while the $p_{1/2}$ zero is moving out. The $p_{3/2}$ zeros behave substantially like the nonrelativistic case (Manson 1985). Thus above $Z = 90$, only the $5p_{1/2}$ photoionisation channel has a zero. This has interesting consequences. For example, the photoelectron angular distribution asymmetry parameter β is rather different depending on whether or not the channel has a zero. Generally, the β values for spin–orbit doublets are rather similar, but not in this case. The values for the 5p subshells of uranium are shown in Fig. 3 where it is clearly seen that the two curves behave rather differently. It can be shown that β is zero at the location of the zero in the p–d channel (Manson 1973). This is seen in the β value for the $5p_{1/2}$ subshell just above 6 a.u. For the $5p_{3/2}$ subshell, the zero appears to be just below threshold. Thus, the existence of separated zeros gives rise to β values which differ by as much as 2 units, just above threshold, which is a very large fraction of the total possible

variation of β (3 units) from -1 to 2. In the threshold region then, the calculation predicts that the photoelectrons from the $5p_{3/2}$ subshell will be rather isotropic, while those from $5p_{1/2}$ will be close to a $\cos^2\theta$ angular distribution.

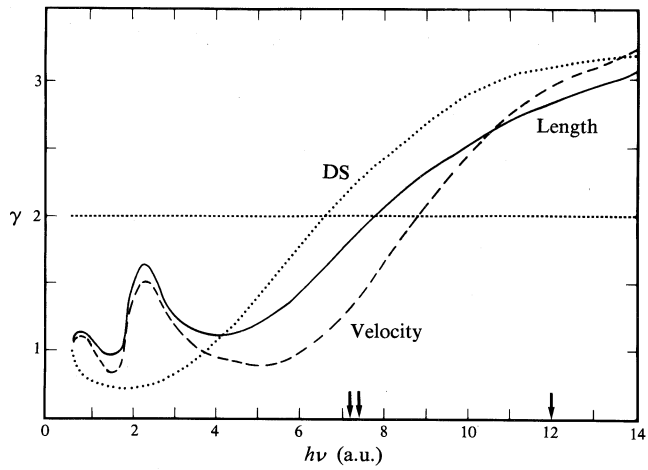

Fig. 4. The $6p_{3/2}$–$6p_{1/2}$ branching ratio for radon, showing the RRPA length and velocity results and the Dirac–Slater (DS) result. The arrows denote the minima in the RRPA calculation; the ones near 7 a.u. are from $6p_{3/2}$ while the one at 12 a.u. is from $6p_{1/2}$. The horizontal dashed line represents the statistical ratio.

In addition, branching ratios are bound to be affected by the location of these zeros. When one channel has a zero, clearly its cross section will be anomalously small compared with a channel that does not have a zero in that vicinity. Returning to Fig. 1, it is seen that for the 6p case, the $p_{3/2}$ zeros are at a much lower energy than those of $p_{1/2}$. Thus the $6p_{3/2}$–$6p_{1/2}$ branching ratio should be smaller than the statistical ratio of 2 at the lower energies, and above 2 at the higher energies. The actual result is shown in Fig. 4 where it is seen that the DS result is as predicted.

All of the relativistic results presented here were calculated using the DS formalism. At this point it is fair to inquire as to the reliability of such results, calculated as they were with approximate exchange and correlation omitted. Since experimental work in this Z region is too sparse for an appeal to experiment to answer the question, we have performed far more accurate relativistic random phase approximation (RRPA) calculations for radon, $Z = 86$. The RRPA calculations include exchange along with a significant amount of correlation (Johnson and Cheng 1979). The results for the 6p branching ratio, in both length and velocity formulations (Starace 1981) are also shown in Fig. 4. Except for a resonance in the threshold region caused by interchannel coupling with the 5d subshell, the structure on the branching ratio is the same as the DS prediction. The arrows in Fig. 4 show the location of the zeros in the RRPA calculation. The splitting between them is almost precisely the same as the DS result, but they are all shifted upward in energy by about 3 a.u. The result of this shift is an overall shift of the branching ratio curve to higher energy. It is thus clear from the comparison that, while the actual positions of the zeros in the

DS calculation may be somewhat inaccurate, the splittings and overall systematics are substantially correct.

3. Concluding Remarks

The results presented herein show the significant effects that relativistic interactions have in one aspect of the photoionisation of high-Z atoms, the splittings and shifts of the zeros in the dipole matrix elements. In addition, some important implications of these zeros were presented involving photoelectron angular distributions and branching ratios. While the effects are confirmed in one case by an RRPA calculation, they have yet to be tested experimentally. Such experimental tests, in a few cases, would be very helpful to our understanding.

Acknowledgment

We thank the U.S. National Science Foundation for supporting this work.

References

Cooper, J. W. (1962). *Phys. Rev.* **128**, 681.
Fano, U., and Cooper, J. W. (1968). *Rev. Mod. Phys.* **40**, 441.
Herman, F., and Skillman, S. (1963). 'Atomic Structure Calculations' (Prentice–Hall: Englewood Cliffs, NJ).
Johnson, W. R., and Cheng, K. T. (1979). *Phys. Rev.* A **20**, 978.
Manson, S. T. (1973). *J. Electron Spectrosc.* **1**, 413.
Manson, S. T. (1976). *Adv. Electron. Electron Phys.* **41**, 73.
Manson, S. T. (1977). *Adv. Electron. Electron Phys.* **44**, 1.
Manson, S. T. (1985). *Phys. Rev.* A **31**, 3698.
Manson, S. T., and Cooper, J. W. (1968). *Phys. Rev.* **165**, 126.
Manson, S. T., Lee, C. J., Pratt, R. H., Goldberg, I. B., Tambe, B. R., and Ron, A. (1983). *Phys. Rev.* A **28**, 2885.
Samson, J. A. R. (1981). *In* 'Handbuch der Physik', Vol. 31 (Ed. W. Mehlhorn), pp. 123–213 (Springer: Berlin).
Starace, A. F. (1981). *In* 'Handbuch der Physik', Vol. 31 (Ed. W. Mehlhorn), pp. 1–12 (Springer: Berlin).
Tambe, B. R., and Manson, S. T. (1984). *Phys. Rev.* A **30**, 256.
Wuilleumier, F. J. (Ed.) (1976). 'Photoionization and Other Probes of Many-electron Interactions' (Plenum: New York).

Manuscript received 3 February, accepted 29 April 1986